REPORT DOCUMENTATION PAGE

AFRL-SR-BL-TR-99-

0093

1. AGENCY USE ONLY (*Leave Blank*)	2. REPORT DATE 1/21/99	3. REPORT TYP. _____ COVERED Final and Progress Report combined (8/1/96-11/30/98)

4. TITLE AND SUBTITLE	5. FUNDING NUMBERS
Collision Dynamics with Stretched Atoms	F49620-96-1-0142

6. AUTHORS
M.R. Flannery

7. PERFORMING ORGANIZATION NAME(S) AND ADDRESS(ES) School of Physics Georgia Institute of Technology Atlanta, GA 30309-0430	8. PERFORMING ORGANIZATION REPORT NUMBER

9. SPONSORING / MONITORING AGENCY NAME(S) AND ADDRESS(ES) AFOSR/NE 801 North Randolph Street, Room 732 Arlington, VA 22203-1977 Dr. Ralph E. Kelley	10. SPONSORING / MONITORING AGENCY REPORT NUMBER

11. SUPPLEMENTARY NOTES

12a. DISTRIBUTION / AVAILABILITY STATEMENT Approved for public release Distribution is unlimited	12b. DISTRIBUTION CODE

13. ABSTRACT (Maximum 200 words)

19990326 025

This Final Report on Grant AFOSR: F49620-96-1-0142 documents:

(a) the research accomplished

(b) the papers published

(c) the invited papers presented at professional scientific conferences and

(d) the awards received during the research period August, 1996 – November, 1998. The research entitled "Collision Dynamics with Stretched Atoms" deals with stretched atoms in collisions with other species (electrons, ions and atoms) and with recombination processes (electron –ion) which produce stretched atoms.

14. SUBJECT TERMS			15. NUMBER OF PAGES
			16. PRICE CODE

17. SECURITY CLASSIFICATION OF REPORT unclassified	18. SECURITY CLASSIFICATION OF THIS PAGE unclassified	19. SECURITY CLASSIFICATION OF ABSTRACT unclassified	20. LIMITATION OF ABSTRACT UL

DTIC QUALITY INSPECTED 4

Contents

3. RESEARCH ACCOMPLISHED AND PAPERS PUBLISHED

The research accomplished deals with two main topics:

(a) stretched atoms in collisions with other species (electrons, ions and atoms)

and

(b) stretched (excited) atoms resulting from electron - ion recombination. The dynamics of stretched atoms has therefore been concerned with collisions and with recombination.

The following research in these two topics has been written up and published.

1. *Recombination at Ultra-low Energies*, by M. R. Flannery and D. Vrinceanu, in **APS Topical Conference on Atomic Processes in Plasmas**, eds. E. Oks and M. S. Pindzola (AIP Press,1998).

2. *The Classical Atomic Form Factor*, by D. Vrinceanu and M. R. Flannery, Physical Review Letters, (1999)

3. *Cross Sections for Electron Excitation of the 2^3S Metastable Level of He into Higher Triplet Levels*, G. A. Pech, M. E. Lagus, L. W. Anderson, C. C. Lin and M. R. Flannery, Phys. Rev. A **55**,(1997), pp. 2842-2856.

4. *Elastic Scattering: Classical*, Quantal and Semiclassical, by M. R. Flannery in **Atomic, Molecular and Optical Physics Reference Book**, ed. G. W. F. Drake (AIP Press, New York, 1996), Chap. 43, pp. 499-525.

5. *Electron-Ion and Ion-Ion Recombination*, by M. R. Flannery, in **Atomic, Molecular and Optical Physics Reference Book**, ed. G. W. F. Drake (AIP Press, New York, 1996), Chap. 52, pp. 605-629.

The first two papers are attached as Appendices A and B of the present report. Publication #3 represented a joint collaboration with the experimental collision group headed by Professor C. C. Lin at the University of Wisconsin on electron - excited atom collisions. The first page of this publication is reproduced in Appendix C. Publications #4 and 5 were fully documented in the final report AFOSR Grant F 49620-94-1-0379, but were only published during the current research period.

4. INVITED PAPERS PRESENTED AT CONFERENCES

The following papers were presented at professional scientific conferences during the period:

1. *Recombination at Thermal and Ultracold energies*, M. R. Flannery, M. R. Flannery, **Invited Paper**, presented at **50th Gaseous Electronic Conference**, Madison, Wisconsin, October 5-9, 1997.

2. *Recombination at Low and Ultralow Temperatures*, M. R. Flannery, M. R. Flannery, **Invited Paper,** presented at **Molecular Ion Physics Workshop,** Oak Ridge National Laboratory, Oak Ridge, Tennessee, February 20-21, 1998.

3. *Recombination at Ultracold Energies*, M. R. Flannery, **Invited Paper**, presented at **Atomic Processes in Plasmas**, 11th Topical APS Conference, Auburn, Alabama, March 22-26, 1998.

4. *Recombination*, M. R. Flannery, **Allis Prize Invited Plenary Lecture**, presented at **American Physical Society (APS) Division of Atomic, Molecular and Optical Physics**, Santa Fe, New Mexico, May 27-30 , 1998.

5. *Three-Body Recombination*, M. R. Flannery, **Allis Prize Invited Plenary Lecture**, presented at **51st Gaseous Electronics Conference**, Maui, Hawaii, October 19-22, 1998.

6. *Three-Body Electron-Ion*, Ion-Ion and Neutral-Neutral Recombination at Thermal and Ultra-Cold energies, M. R. Flannery, **Invited Paper**, presented at **65th Meeting of the Southeastern Section of The American Physical Society**, Miami, Florida, November 13-15, 1998.

5. HONORS AND AWARDS RECEIVED

The following academic and scientific Honors and Awards were received during the period:

* **Doctor of Science** (*honoris causa*): The Queen's University of Belfast, 1998
  Cited: *For distinction as a physicist.*

* **Recipient of the APS Allis Prize** for the Study of Ionized Gases, 1998
  Cited: *For advancing the understanding of recombination processes, in particular for developing a microscopic theory of three-body ionic recombination; and for his novel applications of classical and quantum mechanical methods to the dynamics of atomic, molecular and ionic systems.*

* **Elected Honorary Member:** Royal Irish Academy, 1997
  Cited: *In recognition for his distinguished services in the Section of Science.*

Appendix A

# Recombination at Ultra-low Energies

M. R. Flannery and D. Vrinceanu

School of Physics, Georgia Institute of Technology, Atlanta, GA 30332-0430[1]

Abstract. Three-body electron-ion recombination is described at ultralow electron temperatures T_e. At $4K$, the initial stage involves extremely rapid collisional capture into high Rydberg states $n > 200$ with high angular momentum $l \approx n - 1$ at a rate $\sim T_e^{-4.5}$. This is followed by extremely slow collisional-radiative decay. The key collisional mechanism appears to be collisional l-mixing of the Rydberg atoms A(n) by ions and electrons until sufficiently low l's are attained so as to permit relatively rapid radiative decay to the lowest electronic levels. This sequence is in direct contrast to the sequence of much slower collisional capture at higher T_e followed by the much faster decay of A(n) by electron collisions to lower levels where radiative decay completes the recombination. At ultra-low temperatures, the rate limiting sequence is therefore collisional l-mixing followed by radiative decay in contrast to recombination at much higher energies and electron densities $N_e \sim 10^8$ cm^{-3}, where the rate limiting step is the initial collisional or radiative capture at intermediate $T_e(\sim 1$ eV) and higher T_e (~ 10 eV) respectively.
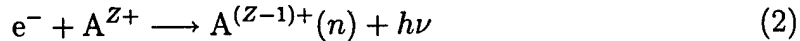
An exact classical solution for l-mixing is obtained.

INTRODUCTION

Three-body collisional capture

$$e^- + A^{Z+} + e^- \longrightarrow A^{(Z-1)+}(n) + e^- \qquad (1)$$

and radiative capture

$$e^- + A^{Z+} \longrightarrow A^{(Z-1)+}(n) + h\nu \qquad (2)$$
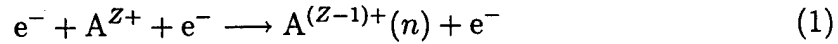
in an electron gas at cryogenic temperatures $T \sim 4K$ and lower are considered. Simple classical expressions for the cross section σ and rate $\alpha \sim Z^3 T_e^{-4.5}$ of (1) are derived. We shall also provide an exact classical solution for the angular momentum mixing $n, l \rightarrow n, l'$ of Rydberg levels by the time varying electric field $\mathcal{E} = -[Z_1 e/R^3(t)]\mathbf{R}(t)$ generated by distant collisions with an ion of charge $Z_1 e$. The work has particular significance to the production of anti-hydrogen at 4 K and to proposed experiments on electron recombination with Rb$^+$ and Xe$^+$ at 5 mK.

RADIATIVE RECOMBINATION

The quantal cross section for photoionization of $A(n, l)$, in conventional notation [1], is

$$\sigma_I(h\nu) = \left\{ \left[\frac{64\alpha}{3\sqrt{3}} (\pi a_0^2) \frac{n}{Z} \right] \left(\frac{I_n}{h\nu} \right)^3 \right\} \frac{2l+1}{n^2} G_{nl}(h\nu) \equiv {}_k\sigma_n(h\nu) \frac{2l+1}{n^2} G_{nl}(h\nu)$$

where ${}_k\sigma_n(h\nu)$ is the semiclassical (Kramers) photoionization cross section [2] and the bound-free Gaunt factor $G_{nl} \sim 1$ and $\omega^{-(l+1/2)}$ as $\omega = h\nu/I_n$ tends to 1 and ∞ respectively. The former limit is appropriate to ultracold ejected electrons while the latter limit indicates that low l' are favored. The detailed balance relation is

$$g_e g_A^+ k_e^2 \sigma_R(E) = g_\nu g_A k_\nu^2 \sigma_I(h\nu)$$

where the statistical weights g_i are $\{2, 1, 2, 2(2l+1)\}$ for e, A^+, $h\nu$ and A, respectively and where $k_\nu^2/k_e^2 = \alpha^2(h\nu)^2/(4EI_H) = (v_0/c)^2(I_H/4E)$ with $I_H = (e^2/2a_0)$. The cross section for radiative recombination of electrons with energy E is then

$$\sigma_R(n) = \left\{ \left(\frac{8\pi a_0^2 \alpha^3}{3\sqrt{3}} \right) \frac{2Z^2 I_H}{E} \right\} \left[\frac{2}{n} \frac{I_n}{(I_n + E)} \right] G_n(E + I_n)$$

which is much smaller by a factor $\mathcal{O}(\alpha^2)$ than σ_I. G_n is the l-averaged Gaunt factor $n^{-2} \sum_{l=0}^{n-1} (2l+1) G_{nl}$. The corresponding rate is

$$\alpha_{RR}(n, T_e) = \langle v_e \rangle \left(\frac{8\pi a_0^2 \alpha^3}{3\sqrt{3}} \right) \left[\frac{2Z^2 I_H}{kT_e} \right] \frac{2}{n} F_n(b_n)$$

with

$$F_n(b_n) = b_n e^{b_n} \int_1^\infty \frac{G_n(\omega)}{\omega} e^{-b_n \omega} \, d\omega$$

where $b_n = I_n/kT_e$ and $\omega = h\nu/I_n$. For ultracold recombination, $G_n \sim 1$ so that

$$\alpha_{RR}(n, T_e \to 0) = \left\{ \langle v_e \rangle \left(\frac{8\pi a_0^2 \alpha^3}{3\sqrt{3}} \right) \left(\frac{2Z^2 I_H}{kT_e} \right) \right\} \frac{2}{n} b_n e^{b_n} \mathrm{E}_1(b_n)$$

$$\stackrel{\text{def}}{=} \alpha_0(T_e) \frac{2}{n} b_n e^{b_n} \mathrm{E}_1(b_n) \tag{3}$$

the semiclassical (Kramers) rate [1] where

$$\alpha_0(T_e) = 5.966 \ 10^{-13} \left(\frac{300}{T_e} \right)^{1/2} Z^2 \ \mathrm{cm^3 s^{-1}}$$

and where E_1 is the first exponential integral $\int_b^\infty e^{-x} \, dx/x$. Since $be^b \mathrm{E}_1$ increases from 0 to 1 as b increases from 0 to ∞, (3) shows that Radiative Recombination favors transitions to low n.

Ultracold Radiative Recombination into the high level n_0 determined by $kT_e = I_n$ then proceeds at the rate

$$\alpha_{RR}(n) = 7.12 \ 10^{-13} \left(\frac{300}{T_e}\right)^{1/2} \frac{Z^2}{n} \ \text{cm}^3\text{s}^{-1}$$

The rate into all levels $n' \geq n$ is

$$\alpha_{RR}(n' \geq n) = \alpha_0(T_e) \int_0^{b_n} e^b \text{E}_1(b) \ db$$

$$= \alpha_0(T_e)[\gamma + \ln b_n + e^{b_n} \text{E}_1(b_n)]$$

where $\gamma = 0.5772$ is the Euler's constant. For $b_n = 1$, then

$$\alpha_{RR}(n' \geq n_0) = 7 \ 10^{-13} \left(\frac{300}{T_e}\right)^{1/2} Z^2 \ \text{cm}^3\text{s}^{-1}$$

The rate into all levels $n' \leq n$ including the effect of cascades [3] is

$$\alpha_{RR}(n' \leq n) = 3.80 \ 10^{-12} \left(\frac{300}{T_e}\right)^{0.63} Z^2 \ \text{cm}^3\text{s}^{-1}$$

COLLISIONAL CAPTURE RATE

The forward recombination and reverse ionization rates α_R and α_I of process (1) are interconnected by detailed balance

$$\tilde{N}_e \tilde{N}(n) \alpha_I(n) = \tilde{N}_e \tilde{N}_+ \alpha_R(n) \tag{4}$$

where the Saha-Boltzmann distribution $\tilde{N}$ of bound levels n in collisional equilibrium with the continuum state distributions $\tilde{N}_e$ and $\tilde{N}_+$ is

$$\frac{\tilde{N}(n)}{\tilde{N}_+ \tilde{N}_0} = \frac{h^3}{(2\pi m_e kT_e)^{3/2}} \ n^2 \exp(I_n/kT_e) \quad ; \quad I_n = Z^2 \frac{I_H}{n^2} \tag{5}$$

where I_n is the ionization energy level n. It is useful to rewrite (5) in the equivalent forms:

$$\frac{\tilde{N}(n)}{\tilde{N}_+ N_e} = Z \ (\pi R_e^2)^{3/2} \ (n^2/n_0^2) \exp(n_0^2/n^2) \quad ; \quad I_n/kT_e = n_0^2/n^2 \tag{6}$$

in terms of the characteristic Coulomb Radius $ZR_e = Z(e^2/kT_e) = 2n_0^2(a_0/Z)$, and

$$\frac{\tilde{N}(n)}{\tilde{N}_+ N_e} = \frac{Z}{2} \ (\pi R_e^2)^{3/2} \ b_n^{-5/2} \frac{db_n}{dn} \ \exp(b_n) \quad ; \quad b_n = I_n/kT_e \tag{7}$$

where $db_n/dn = (2b_n)/n$. The distribution (6) exhibits a minimum at $n = n_0$ which corresponds to $b_n = 1$.

The rate for ionization of $A(n)$ by electrons of energy E is

$$\alpha_I(n) = \langle v_e \sigma_I(E) \rangle = \langle v_e \rangle \int\limits_0^\infty \epsilon \, e^{-\epsilon} \, \sigma_I(\epsilon) \, d\epsilon \quad ; \quad \epsilon = E/kT$$

A. Detailed Balance Rate: The Thomson collisional cross section [4]

$$\sigma_I(E) = \pi e^4 \frac{Z^2}{E} \left(\frac{1}{E} - \frac{1}{I_n} \right) = \pi R_e^2 \frac{Z^2}{\epsilon} \left(\frac{1}{b_n} - \frac{1}{\epsilon} \right) \tag{8}$$

for electron ejection from the Rydberg $A(n)$, yields the rate of ionization

$$\alpha_I(n) = Z^2 \pi R_e^2 \langle v_e \rangle \frac{e^{-b_n}}{b_n} \left(1 - b_n e^{b_n} \mathrm{E}_1(b_n) \right)$$

From detailed balance (4) and (7), the rate of collisional capture into level n is then:

$$\alpha_{CC}(n) = Z^3 (\pi R_e^2)^{5/2} \langle v_e \rangle \, N_e \, (n b_n^{5/2})^{-1} [1 - b_n e^{b_n} \mathrm{E}_1(b_n)] \tag{9}$$

The factor multiplying [ ] in (9) varies as $Z^3 n^4 T_e^{-2}$. Since $b e^b \mathrm{E}_1(b) \to 1 - b^{-1}$ for very large b then $\alpha_{CC} \sim Z^3 n^6 T_e^{-1}$ at ultracold energies when $kT_e \ll I_n$.

Recombination into all levels $\Sigma \leq n$ proceeds at a rate

$$\alpha_{CC}(\Sigma) = \sum_{n'=1}^{n} \alpha_{CC}(n') \approx \int\limits_1^n \alpha_{CC}(n') \, dn' = \int_{b_n}^{b} \alpha_{CC}(n) \frac{n}{2 b_n} \, db_n \tag{10}$$

where $b = I_1/kT_e$ can be replaced by infinity since $b_1 \gg b_n$. Then

$$\alpha_{CC}(\Sigma) = \frac{Z^3}{2} (\pi R_e^2)^{5/2} \langle v_e \rangle \, N_e I(b_n) \tag{11}$$

where

$$I(b_n) = \int\limits_{b_n}^\infty \frac{1 - b_n e^{b_n} \mathrm{E}_1(b_n)}{b^{7/2}} \, db$$

Since

$$R_e^{5/2} \langle v_e \rangle \equiv \frac{8.094 \, 10^{-9}}{T(K)^{4.5}} = 5.769 \, 10^{-20} \left(\frac{300}{T(K)} \right)^{4.5}$$

$$= \frac{5.144 \, 10^{-27}}{E_{eV}^{4.5}} = \frac{4.070 \, 10^{-32}}{E_{Ry}^{4.5}}$$

for T_e expressed in different units, then

$$\alpha_{CC}(\Sigma) = 6.71 \ 10^{-20} N_e \left(\frac{300}{T_e}\right)^{4.5} R(b_n) \tag{12}$$

which exhibits the characteristic $Z^3 T_e^{-4.5}$ dependence [5]. The function is $R(b_n) = I(b_n)/I(1)$. Since the equilibrium distribution (7) exhibits a maximum at $kT_e = I_n$, where $n = n_0$ or $b_n = 1$, there is a bottleneck at $n = n_0$ and it may be argued that all levels $n \geq n_0$ are collisionally connected with the continuum and may be regarded as subject to re-ionization alone, while levels $n \leq n_0$ are connected mostly with lower bound levels and are therefore subject only to further de-excitations. Then R in (12) is unity.

In terms of this bottleneck level n_0,

$$ZR_e = 2n_0^2 (a_0/Z) \quad ; \quad \langle v_e \rangle = \left(\frac{2}{\pi}\right)^{1/2} (Zv_0/n_0)$$

Then (9) provides the CC-rate into level n_0 as

$$\alpha_{CC}(n_0) = 64 \ \pi^2 \ Z^{-6} \ n_0^8 (a_0^2 v_0)(N_e a_0^3) \ \{[1 - eE_1(1)] = 0.4\}$$

and (11) the CC-rate into all levels $n \leq n_0$ as

$$\alpha_{CC}(n \leq n_0) = 32 \ \pi^2 n_0^9 (a_0^2 v_0)(N_e a_0^3) \ \{I(1) = 0.1329\} \tag{13}$$

The strong n_0-dependencies are therefore highlighted. Since $n_0^2 \sim Z^2/kT_e$, the $Z^3 T_e^{-4.5}$ dependence of (11) is recovered from (13). Although the Thomson cross section (8) can be replaced by a variety of cross sections derived from more elaborate binary-encounter classical theory, the key dependence $Z^3 T_e^{-4.5}$ is still preserved. Allowance for the discrete n' summation rather than the continuous integration in (10) shows that $\alpha_R(n)/2$ is simply added to (11).

B. Direct CC Rate: In the three-body CC (1), some of the energy gained by the incident (test) electron 1 moving with total energy $E_1 = (3/2)kT_e$ and kinetic energy $T_1(R) = 3/2kT_e + |V_{13}(R)|$ in the field of the ion 3 with charge Ze is lost upon repulsive Coulomb collision with an ambient (field) electron 2 of average energy $E_2 = (3/2)kT_e$ in an electron gas bath at temperature T_e. For (1-2) scattering by angle Ψ in the (1-2) CM, the energy in the laboratory (fixed ion 3) frame lost by 1 to 2 is

$$\Delta E = [T_1(R) - E_2] \sin^2 \frac{\Psi}{2} = |V_{13}(R)| \sin^2 \frac{\Psi}{2}$$

In order that the total energy of 1 is changed from E_1 to all bound energies $E_1' \leq -\epsilon_0 kT_e$, the (1-2) scattering must satisfy

$$|V_{13}(R)| \sin^2 \frac{\Psi}{2} \geq (\frac{3}{2} + \epsilon_0)kT_e \tag{14}$$

In a repulsive Coulomb (1-2) encounter

$$\sin^2 \frac{\Psi}{2} = \frac{b_c^2}{b^2 + b_c^2} \quad , \quad b_c = \frac{e^2}{2E_{rel}}$$

where E_{rel} is the energy of (1-2) relative motion which, on average, is $3/2kT_e$. Condition (14) then provides the averaged cross section

$$\sigma_{12}(R) = \frac{1}{9}\pi R_e^2\left(\frac{R_0}{R} - 1\right) \quad , \quad R_0 = \frac{ZR_e}{\epsilon_0 + 3/2}, \quad R_E = \frac{e^2}{kT_e} \qquad (15)$$

for the formation of bound states with energy $E_1' \leq -\epsilon_0 kT_3$ by (e - e) collisions at test-electron - ion separation $R \leq R_0$. For $R \geq R_0$, σ_{12} vanishes. When $\epsilon_0 = 0$, R_0 is the Thomson trapping radius [1]. The collisional capture cross section at total energy

$$E = \frac{1}{2}m_e v^2(R) + V_{13}(R) = \frac{1}{2}m_e\dot{R}^2 + V_{13}(R) + 2m_e E\frac{\rho^2}{R^2}$$

is

$$\sigma_{CC}(E) = 2\pi \int\limits_0^\infty \rho d\rho \int\limits_{-\infty}^\infty W(R,E)\, dt \qquad (16)$$

where $W(R,E)\,dt$ is the probability of the energy-reducing (1-2) collision occuring within the time interval $dt = dR/v_R(R)$ about $R(t)$ of (1-3) trajectory, so that

$$\sigma_{CC}(E) = 4\pi \int\limits_0^\infty \rho d\rho \int\limits_{R_i(\rho)}^\infty W(R,E)\, \frac{dR}{\dot{R}}$$

where R_i is the orbit's pericenter at which $\dot{R} = 0$. On reversing the order of integration,

$$\sigma_{CC}(E) = 2\pi \int\limits_{R_i(0)}^\infty W(R,E)\, dR \int\limits_0^{\rho_1} \frac{d\rho^2}{\dot{R}(E,E)}$$

where $\rho_1^2(R,E) = R^2[1 - V(R)/E]$ gives the maximum impact parameter ρ_1 that can just acces the point R. For purely atractive interactions $R_i(0) = 0$ and $V = E$ at $R_i(0)$ when repulsion occurs at zero impact parameter. Since

$$\int\limits_0^{\rho_1} \frac{d\rho^2}{\dot{R}(R,E)} = \frac{2R^2}{v(R)}[1 - \frac{V_{13}(R)}{E}]$$

then

$$\sigma_{CC}(E) = 4\pi \int\limits_{R_i(0)}^\infty \frac{W(R,E)}{v(R)}[1 - \frac{V_{13}(R)}{E}]\, dR$$

The (1-2) collision probability within an element ds of the (1-3) orbit is

$$W(R,E)\, dt = \frac{ds}{\lambda} = N_e\sigma_{12}(R)v(R)\, dt$$

where λ is the free path length towards collision. Hence (16) reduces exactly to

$$\sigma_{CC}(E) = 4\pi N_e \int_0^{R_0} \sigma_{12}(R) \left(1 - \frac{V_{13}(R)}{E}\right) R^2 \, dR$$

which with (15) and $V_{13}(R) = -Ze^2/R$, yields

$$\sigma_{CC}(E = \epsilon kT) = \frac{4}{27}\pi^2 Z^3 R_e^5 N_e \left[\frac{1 + 3(\epsilon_0 + 3/2)/\epsilon}{2(\epsilon_0 + 3/2)^3}\right] \tag{17}$$

The factor $Z^3 R_e^3$ originates from the reaction volume R_0^3 while the additional R_e^2 originates from the (1-2) scattering cross section (15).

The associated collisional capture rate

$$\alpha_{CC} = \langle v_e \rangle \int_0^\infty \sigma_{CC}(\epsilon)\epsilon e^{-\epsilon} \, d\epsilon$$

is then

$$\alpha_{CC}(\epsilon_0) = \frac{4}{27}\pi^2 Z^3 \langle v_e \rangle R_e^5 N_e \left[\frac{3}{2}\frac{\epsilon_0 + 11/6}{(\epsilon_0 + 3/2)^3}\right]$$

The rate for production of all levels $\leq -kT_e$ is therefore

$$\alpha_{CC}(1) = 2.29 \, 10^{-20} \left(\frac{300}{T_e}\right)^{4.5} N_e \tag{18}$$

which is in excellent agreement with the Monte-Carlo result of Mansbach and Keck [5] and a factor of 3 lower than the detailed balance rate (12) derived from the Thompson ionization cross section (8). This simple result $\sim Z^3 T_e^{-4.5}$ is preserved even in elaborate classical treatments of the ionization [6] or of the recombination [7] with correct averaging of the dynamical quantities .

The frequencies $\nu_{CC} = \alpha_{CC} N_e$ and $\nu_{RR} = \alpha_{RR} N_e$ are compared in Table (1) at various T_e for typical $N_e \approx 10^8$ cm^{-3}. Since $\nu_{CC}/\nu_{RR} \sim N_e/T_e^4$ it is seen that Collisional Capture dominates Radiative Recombination at cryogenic and lower T_e by large factors $\sim 10^7$. Also CC $\approx$ RR at $T_e \sim 300$K while CC $\ll$ RR at 1eV.

TABLE 1. Collisional Capture and Radiative Recombination frequencies for different temperatures

T_e	$\nu_{CC}(s^{-1})$	$\nu_{RR}(s^{-1})$
4 K	6.3×10^4	5.8×10^{-3}
300 K	2.3×10^{-4}	3.8×10^{-4}
1 eV	2.0×10^{-11}	3.9×10^{-5}

RADIATIVE DECAY RATES

Level i decays radiatively to level j at a rate

$$A(i \to j) = \frac{1}{6} A_0 (E_{ij}/I_H)^3 (S_{ij}^{au}/g_i)$$

where the line strength S_{ij} in a.u. is $\sum_{\alpha,\alpha'} |\langle nlm|\vec{r}|n'l'm'\rangle|^2$ and $A_0 = \alpha^3/t_0 = 1.604 \, 10^{10} \, s^{-1}$ where t_0 is the a.u. of time $(e^2/a_0)/\hbar$. Level nl decays to all lower levels s at frequency

$$\nu_r(nl) = \sum_{s<n} A(nl \to s, l+1)$$

$$= \frac{2}{3} Z^4 A_0 \left[\frac{1}{n^3(l+\frac{1}{2})^2} \to \left\{ \begin{array}{ll} n^{-5} & , \text{for } l = n-1 \\ 4/9 \, n^{-3} & , \text{for } l = 1 \end{array} \right] \right.$$

The circular ($l = n-1$) states, mainly populated by collisional capture (CC), are therefore very long lived and decay at frequency

$$\nu_r(n, l = n-1) \approx \frac{10^{10}}{n^5} \quad \ll \quad \nu_r(np \to 1s) \approx \frac{4}{9} \frac{10^{10}}{n^3} \, (s^{-1})$$

very much less than that for the $(np \to 1s)$ transition. The levels $n_0 \approx 200$ populated by CC at 4K have therefore a long radiative lifetime $\tau_r \sim 32$ s when compared with $2 \, 10^{-3}$ for the $(n_0 p \to 1s)$ transition. The overall rate of recombination via capture into level n followed by radiative decay is

$$\alpha \sim \frac{\nu_C \nu_r}{\nu_C + \nu_r}$$

where $\nu_C = \nu_{CC} + \nu_{RR}$. Since the radiative decay frequencies for $n \approx n_0$ are much less than the frequency $\alpha_{CC} N_e^2$ for collisional capture at ultralow temperatures, the overall recombination rate is controlled by the limiting rate ν_r. The question now addressed is the further effect of collisions between Rydberg atoms and ambient electrons and ions.

INELASTIC COLLISIONS AND STARK MIXING

Three important frequencies or timescales in the collision, depicted in Figure (1) are:

(A) The projectile Rotation (Collision) Frequency ω_R of the Projectile

$$\omega_R = \dot{\Phi} = \frac{bv}{R^2} \xrightarrow{\text{large b}} \frac{v}{b} \quad \approx \quad \frac{1}{\tau_{coll}}$$

(B) The Transition (Orbital) Frequency ω_n of the Rydberg electron:
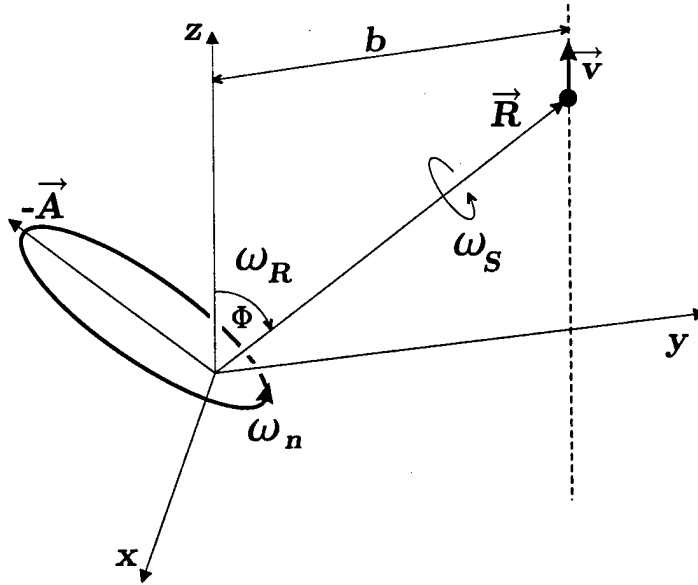
$$\omega_{ij} = \frac{E_i - E_j}{\hbar}$$

FIGURE 1. The three important frequencies in the Rydberg projectile collision

which for transitions $n \to n-1$ between neightboring levels is simply $\omega_{n,n-1} = \omega_0/n^3 = \omega_n = v_n/a_n$, the orbital frequency, where $a_n = n^2 a_0/Z$ and $v_n = Z v_0/n$.

(C) **The Stark Precession Frequency** ω_S for precession of **A** about **R**: Under the ion Electric Field $\mathcal{E} = Z_1 e/R^2$ the Stark frequency

$$\omega_S = \frac{3}{2} \frac{a_n}{n\hbar} (e\mathcal{E}) = \frac{3}{2} \frac{Z_1 a_n v_n}{R^2}$$

provides the precessional frequency of the Runge-Lenz (eccentricity) vector **A** of the Rydberg orbit about the field direction.

By considering the $\exp(i\omega t)$ factor in time dependent perturbation theory, the following types of collisions can be characterized as in [8].

1. Orbital Adiabatic: $\omega_R \ll \omega_n$

$$\frac{b}{a_n} \gg \frac{v}{v_n}$$

where the orbital electron adjust itself adiabatically to the ion perturbation and no transitions occur.

2. Orbital Sudden: $\omega_R \gg \omega_n$

$$\frac{b}{a_n} \ll \frac{v}{v_n}$$

which causes inelastic $(n \to n')$ transitions

3. Stark Adiabatic: $\omega_R \ll \omega_S$

$$\frac{bv}{R^2} \ll \frac{3}{2} \frac{Z_1 a_n v_n}{R^2}$$

$$\frac{b}{a_n} \ll \frac{3}{2}\frac{Z_1 v_n}{v}$$

where elastic collisions occur.

4. Stark Sudden: $\omega_R \gg \omega_S$

$$\frac{b}{a_n} \gg \frac{3}{2}\frac{Z_1 v_n}{v}$$

which causes l-mixing $(nl \to nl')$ transitions.

5. The weak Field Condition $\omega_S \ll \omega_n$ i.e., the Stark splitting $\hbar\omega_S \ll \Delta E_{n,n-1}$ implies that $e\mathcal{E} \ll 2/3(e^2/a_n^2)$ so that the collision occurs for distant encounters at $R \gg a_n$, the Rydberg radius, for fields $e\mathcal{E} = Z_1 e^2/R^2$. The electron's orbital time is then much shorter than any characteristic time to cause changes to the elliptical orbit. The vectors **A** and angular momentum **L** which are constant for the unperturbed motion become good dynamical variables for the description of the perturbed motion.

With respect to orbital motion, the collision is sudden or adiabatic according to $b < b_C$ and $b > b_C$, respectively, where $b_C = (v/v_n)a_n$. With respect to the Stark frequency, collision is adiabatic or sudden according to $b < b_S$ and $b > b_S$, respectively, where $b_S = (v_n/v)a_n$. The impact parameter b-space can then be partitioned according to:

$$b_s = \tfrac{3}{2}\frac{Z_1 v_n}{v}a_n$$
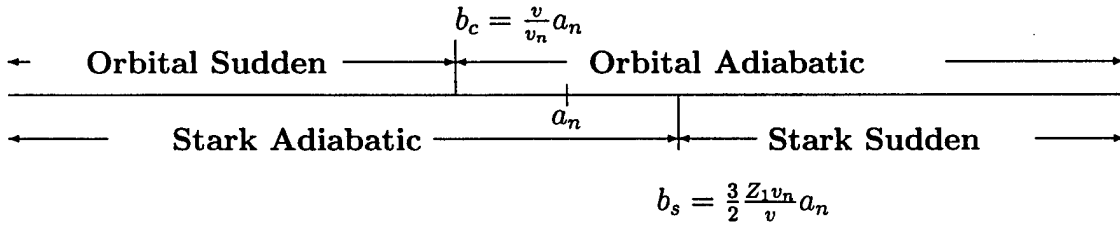
As v decreases, b_S increases outward and b_C increases inward, thereby limiting the extent of the sudden regions where n changes and l-mixing occurs. The (v, b)-phase space can be partitioned into the four characteristic regions illustrated in Figure (2). For $v > v_n$, the (n, l) changing and l changing (Orbital and Stark Sudden) shaded regions overlap and expand, in direct contrast to ultracold speeds $v \le v_n$ where the Orbital and Stark Adiabatic (clear) regions increase and the shaded regions diminish and do not overlap indicating few collisional changes.

CLASSICAL THEORY OF STARK MIXING COLLISIONS

In addition to the energy E_n and angular momentum **L** of an unperturbed Rydberg electron moving with velocity **v** in an elliptical orbit with eccentricity
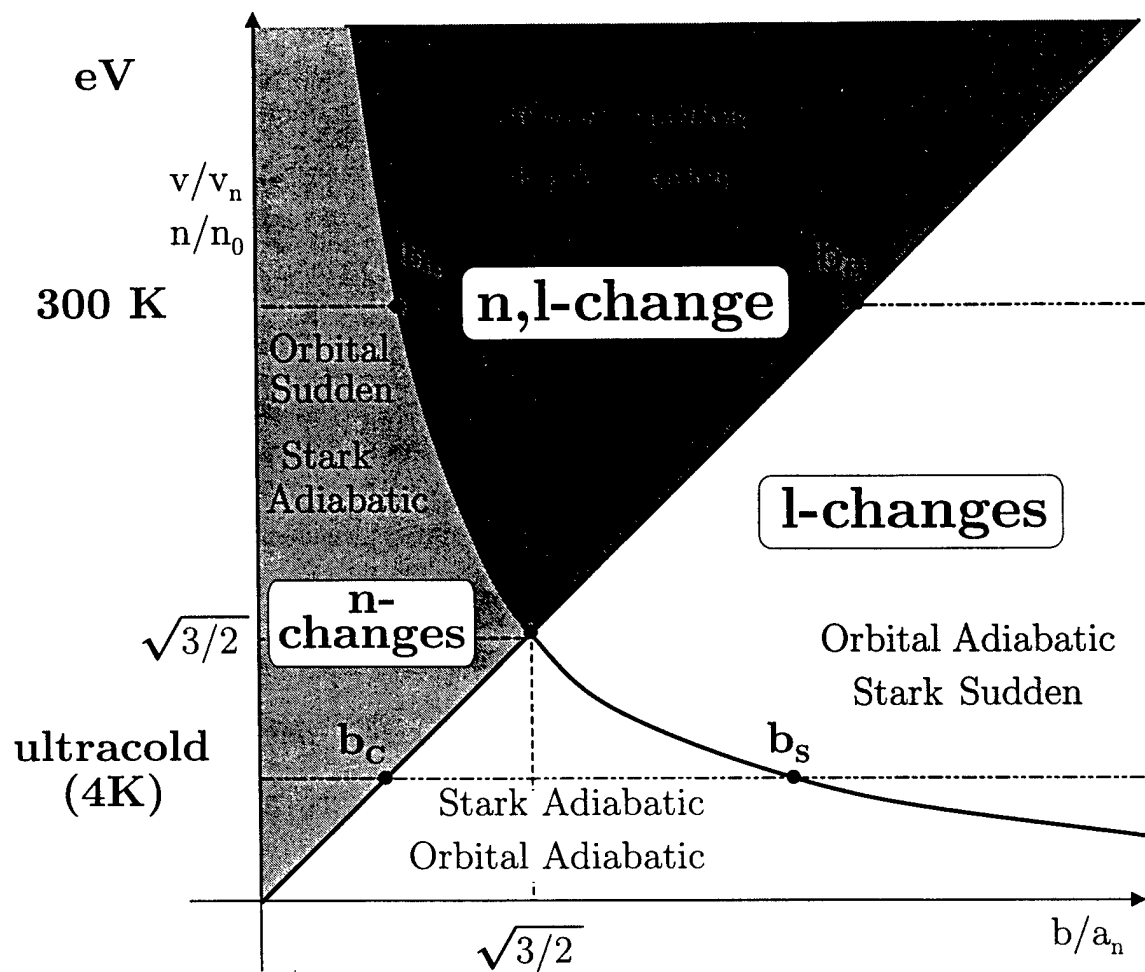
FIGURE 2. Partitioning the v-b phase space map into 4 regions characterized mainly by: (a) energy changes, (b) energy and angular momentum changes, (c) angular momentum changes and (d) no changes under the weak field condition (5)

$\epsilon = (1 - L^2/ma_nk)^{1/2}$ and semi-major axis $a_n = k/2|E_n|$ in the field $-k/r$, the Runge-Lenz (or eccentricity) vector

$$\mathbf{A} = v_n^{-1}[\mathbf{v} \times \mathbf{L} - \frac{k}{r}\mathbf{r}]$$

$$v_n = \langle v^2 \rangle^{1/2} = \frac{Zv_0}{n} \qquad k = Ze^2 \qquad v_0 = \frac{e^2}{\hbar}$$

directed toward the pericenter and normalized to angular momentum units is also conserved in magnitude $A = (ma_nk)^{1/2}\epsilon$ and direction. Moreover $\mathbf{A} \cdot \mathbf{L} = 0$ and $A^2 + L^2 = ma_nk = n^2\hbar^2$. The dipole classically averaged over the orbit time is

$$\mathbf{d} = -e\langle \mathbf{r} \rangle = \frac{3e}{2}(a_n\epsilon) = \frac{3e}{2}\frac{\mathbf{A}}{mv_n}$$

In a.u., $A^2 = n^2 - (l + 1/2)^2$ and the dipole $\mathbf{d} = (3/2)n\mathbf{A}$ is maximum $3/2n^2$ for highly eccentric orbits $l \approx 0$ and is vanishingly small for circular orbits ($l \lesssim n$). In presence of an electric field of intensity $\boldsymbol{\mathcal{E}}$, the angular momentum $\mathbf{L}$ changes at the rate

$$\frac{d\mathbf{L}}{dt} = -e\mathbf{r} \times \boldsymbol{\mathcal{E}}$$

so that the change of $\mathbf{L}$ (classically) averaged over one orbital period T is given by

$$\frac{\Delta \mathbf{L}}{T} = \langle \frac{d\mathbf{L}}{dt} \rangle = -\frac{e}{T}\int_0^T (\mathbf{r} \times \boldsymbol{\mathcal{E}})\, dt$$

Approximation 1: Assume that the perturbation is adiabatic ($\omega_R \ll \omega_n$) with respect to the orbital frequency ω_n. Then $\langle \mathbf{r} \times \boldsymbol{\mathcal{E}} \rangle = \langle \mathbf{r} \rangle \times \langle \boldsymbol{\mathcal{E}} \rangle$ so that

$$\frac{\Delta \mathbf{L}}{T} = -\boldsymbol{\omega}_S \times \mathbf{A}$$

in terms of the Stark frequency

$$\boldsymbol{\omega}_S(t) = \frac{3}{2}\frac{e\langle \boldsymbol{\mathcal{E}} \rangle}{mv_n} = \frac{3}{2}\left(\frac{a_n}{n\hbar}\right)e\langle \boldsymbol{\mathcal{E}} \rangle$$

which is $3n\langle \boldsymbol{\mathcal{E}}_{au} \rangle/2$ in a.u.

Approximation 2: Assume also that $\langle \boldsymbol{\mathcal{E}} \times \mathbf{L} \rangle = \langle \boldsymbol{\mathcal{E}} \rangle \times \langle \mathbf{L} \rangle$ for slowly varying $\boldsymbol{\mathcal{E}}$. It can be shown that the change $\mathbf{A}$ over one period is

$$\frac{\Delta \mathbf{A}}{T} = \langle \frac{d\mathbf{A}}{dt} \rangle = -\boldsymbol{\omega}_S \times \mathbf{L}$$

Approximation 3: Replace the changes $\Delta \mathbf{L}$ and $\Delta \mathbf{A}$ over one period by $\dot{\mathbf{L}}T$ and $\dot{\mathbf{A}}T$ to give the set of coupled equations

$$\frac{d\mathbf{A}}{dt} = -\boldsymbol{\omega}_S(t) \times \mathbf{L} \qquad \frac{d\mathbf{L}}{dt} = -\boldsymbol{\omega}_S(t) \times \mathbf{A}$$

where ω_S tracks the time variation of the electric field in magnitude and direction.

Under the substitution

$$X = \frac{L + A}{2} \qquad Y = \frac{L - A}{2} \tag{19}$$

the above set of differential equations becomes decoupled to yield

$$\frac{dX}{dt} = -\omega_S(t) \times X \qquad \frac{dY}{dt} = +\omega_S(t) \times Y \tag{20}$$

where $X^2 = Y^2 = (L^2 + A^2)/4 = n^2\hbar^2/4$. The classical analysis for constant electric fields is given Born in [9]. For time independent ω_S, both X and Y precess with constant frequency ω_S about the (fixed) direction of ω_S. For general time-varying ω_S, the system of differential equations (20) does not have an exact solution. Percival and Richards [8] have used classical perturbation theory to solve (20) and then provided a diffusional theory of angular momentum mixing. Bellomo et al [10] approached the same problem by proceeding via the time evolution propagator $U_{rot}^{\pm}(t, t_0)$ for X and Y in the rotating frame, an approach which results in formulae too complicated for physical changes ΔL and ΔA to be extracted.

An **Exact Analytical Solution** is however possible when the external time dependence of $\omega_S(t)$ is provided by the electric field $\mathcal{E} = Z_1 e(-\hat{R})/R^2$ of a projectile ion or electron of charge $Z_1 e$ passing the Rydberg atom at large distances $R \gg a_n$, the condition for the weak field approximation. Then

$$\omega_S(t) = -\frac{3}{2}\left(\frac{Z_1 e^2}{m v_n}\right)\frac{\hat{R}(t)}{R^2(t)} = -\frac{3}{2}\left(\frac{Z_1}{Z}\right)\left(\frac{a_n v_n}{R^2(t)}\right)\hat{R}(t)$$

which varies in both magnitude and direction. Since the vector R rotates at the frequency

$$\omega_R(t) = -\frac{d\Phi}{dt}\,\hat{\imath} = \frac{vb}{R^2(t)}\,\hat{\imath}$$

then the vector

$$\alpha(t) = \frac{\omega_S}{\omega_R} = \frac{3}{2}\left(\frac{Z_1}{Z}\right)\frac{a_n v_n}{bv}\,\hat{R}(t)$$

has the constant magnitude $3/2(Z_1/Z)(\tilde{b}\tilde{v})^{-1}$ for a particle with *reduced* speed $\tilde{v} = v/v_n$ in a given trajectory of reduced impact parameter $\tilde{b} = b/a_n$. Since the value $\alpha = 1$ separates the Stark Sudden ($\alpha \ll 1$) and the Stark Adiabatic ($\alpha \gg 1$) regions at $b = b_S$ (see Figure (2)), we refer to α as the Stark parameter. This suggests that Φ could be a more useful variable instead of time t. Hence the first equation in (20) is

$$\frac{dX}{d\Phi} = \frac{dX}{dt}\frac{d\Phi}{dt} = \alpha(0, \sin\Phi, \cos\Phi) \times X \tag{21}$$

Since the tip of X moves on the surface of a sphere, the solution of this equation, the final X vector (corresponding to $t \to \infty$ or $\Phi = 0$), is a rotation of the initial

X vector (corresponding to $t \to -\infty$ or $\Phi = \pi$). The second equation in (20) has a similar solution. The exact form of the resulting rotation matrices are presented in the Appendix. As a result of the collision the vectors **L** and **A** change to

$$
\begin{bmatrix} \tilde{L}_1 \\ \tilde{L}_2 \\ \tilde{L}_3 \end{bmatrix} = \frac{1}{\gamma^2} \begin{bmatrix} 1 + \alpha^2 \cos(\pi\gamma)L_1 & -\alpha^2\gamma\sin(\pi\gamma)A_2 & \alpha(-1+\cos(\pi\gamma))A_3 \\ \gamma^2\cos(\pi\gamma)L_2 & \gamma\sin(\pi\gamma)L_3 & -\alpha\gamma\sin(\pi\gamma)A_1 \\ \gamma\sin(\pi\gamma)L_2 & -(\alpha^2+\cos(\pi\gamma))L_3 & \alpha(1-\cos(\pi\gamma))A_1 \end{bmatrix} \quad (22)
$$

and

$$
\begin{bmatrix} \tilde{A}_1 \\ \tilde{A}_2 \\ \tilde{A}_3 \end{bmatrix} = \frac{1}{\gamma^2} \begin{bmatrix} (1 + \alpha^2 \cos(\pi\gamma))A_1 & -\alpha^2\gamma\sin(\pi\gamma)L_2 & \alpha(-1+\cos(\pi\gamma))L_3 \\ -\gamma^2\cos(\pi\gamma)A_2 & \gamma\sin(\pi\gamma)A_3 & \alpha\gamma\sin(\pi\gamma)L_1 \\ \gamma\sin(\pi\gamma)A_2 & -(\alpha^2+\cos(\pi\gamma))A_3 & \alpha(1-\cos(\pi\gamma))L_1 \end{bmatrix}
$$

$$(23)$$

where $\gamma = \sqrt{1 + \alpha^2}$ and the components of the initial and final vectors (**L**, **A**) and ($\tilde{\textbf{L}}$, $\tilde{\textbf{A}}$) are defined in the fixed coordinate frame of Figure (1). It easy to check that the above exact solutions satisfy the invariant relations

$$
\tilde{\textbf{L}} \cdot \tilde{\textbf{A}} = \textbf{L} \cdot \textbf{A} = 0
$$

and

$$
\tilde{\textbf{L}}^2 + \tilde{\textbf{A}}^2 = \textbf{L}^2 + \textbf{A}^2 = n^2\hbar^2
$$

The new $(n, \tilde{\textbf{L}})$ orbit is confined to a plane perpendicular to the new $\tilde{\textbf{L}}$ and the energy is preserved (n is not changed). The key to the present exact solutions of (20) for a non-uniform rotating field is provided by the recognition that Φ is a more useful variable than time t and by the Rotation Matrix Algebra (in the Appendix).

In the Stark Sudden region, the Stark parameter α is $\ll 1$. In this limit, the solutions have the simpler form

$$
\begin{bmatrix} \tilde{L}_1 \\ \tilde{L}_2 \\ \tilde{L}_3 \end{bmatrix} = \begin{bmatrix} (1-2\alpha^2)L_1 - 2\alpha A_3 \\ L_2 + \pi\alpha^2/2\, L_3 \\ (1-2\alpha^2)L_3 - \pi\alpha^2/2\, L_2 + 2\alpha A_1 \end{bmatrix}
$$

and

$$
\begin{bmatrix} \tilde{A}_1 \\ \tilde{A}_2 \\ \tilde{A}_3 \end{bmatrix} = \begin{bmatrix} (1-2\alpha^2)A_1 - 2\alpha L_3 \\ A_2 + \pi\alpha^2/2\, A_3 \\ (1-2\alpha^2)A_3 - \pi\alpha^2/2\, A_2 + 2\alpha L_1 \end{bmatrix}
$$

The magnitude of the final angular momentum (for $\alpha \ll 1$) is then

$$
\tilde{\textbf{L}}^2 = \textbf{L}^2 + 4\alpha(-A_3L_1 + A_1L_3) + 4\alpha^2(\textbf{A}^2 - A_2^2 - \textbf{L}^2 + L_2^2)
$$

On retaining only the first order term in α

$$
\tilde{\textbf{L}}^2 \approx \textbf{L}^2 + 4\alpha(\textbf{A} \times \textbf{L}) \cdot \hat{y} = \textbf{L}^2 + 4\alpha AL\cos\xi
$$

where ξ is the angle between $\hat{\mathbf{A}} \times \hat{\mathbf{L}}$ and the Oy axis (Figure (1)).

Since the vectors $\mathbf{A}$ and $\mathbf{L}$ are always orthogonal, the angle ξ is then uniformly distributed over the range $(0, \pi)$ if $\mathbf{L}$ is uniformly distributed on the sphere with radius L, as for an equilibrium distribution of magnetic m-sublevels. The initial L-states then evolves to the final $\tilde{L}$ states with angular momentum distributed according to

$$\mathcal{F}(\tilde{L}) \, d\tilde{L} = \frac{1}{\pi} \, d\xi = \frac{2}{\pi} \frac{\tilde{L}}{\sqrt{(4\alpha AL)^2 - (\tilde{L}^2 - L^2)^2}} \, d\tilde{L}$$

In fact $\mathcal{F}$ can be identified with $W_{L \to \tilde{L}}$, the transition probability density for $L \to \tilde{L}$ transitions.

For arbitrary α, the transition probability W has in general not a simple form. It is however important to recognize that the probability W depends on the projectile velocity v and impact parameter b only via the Stark parameter $\alpha = 3Z_1 n / 2Zvb$.

The cross section for l-mixing in the the Rydberg atom is now

$$\frac{d\sigma}{d\tilde{L}} = 2\pi \int_{b_S}^{\infty} W_{L \to \tilde{L}} \, b \, db = 2\pi \left(\frac{a_n}{\tilde{v}_n}\right)^2 \left(\frac{3Z_1}{2Z}\right)^2 \int_0^1 \frac{1}{\alpha^3} W_{L \to \tilde{L}}(\alpha) \, d\alpha$$

where the α-integral is independent of the speed of the projectile and the Rydberg level n. This general result (where I is the above mentioned integral)

$$\frac{d\sigma}{d\tilde{L}} = 2\pi a_0^2 \left(\frac{3nv_0}{2v}\right)^2 \left(\frac{Z_1}{Z}\right)^2 I$$

is in agreement with the behavior of a normalized Born approximation presented in the recent review [11].

SUMMARY

In addition to providing radiative and collisional rates, the three main points of this paper are:

- Development of a simple classical expression for the cross section (16) and rate (18) of the three-body collisional capture (CC) into level n. The result agrees with the Monte-Carlo trajectory calculations [5] and preserves the $Z^3 T_e^{-4.5}$ dependence of α.

- Presentation of an exact classical analytical solution for the changes $\Delta\mathbf{L}$ and $\Delta\mathbf{A}$ in the angular momentum $\mathbf{L}$ and Runge-Lenz vector $\mathbf{A}$ of a Rydberg atom in the time varying electric field $\mathcal{E} = -Z_1 e \hat{R}(t) / R^2(t)$.

- Pointing out that recombination at ultracold temperatures proceeds by very rapid three-body collisional capture into levels nl, with high l, followed by angular momentum mixing by collisions mainly with ions. Recombination then becomes stabilized by radiative decay of the lower l-levels so produced. This sequence is in direct contrast to recombination at $T_e \gtrsim 1$ eV where collisional and radiative capture are generally the rate limiting steps.

APPENDIX: ROTATION MATRIX ALGEBRA

For a given direction $\hat{n}$, rotate vector $\mathbf{x}$ by angle ϕ about the fixed direction $\hat{n}$ to give

$$\mathbf{x}' = \cos\phi\,\mathbf{x} + (1 - \cos\phi)(\hat{n}\cdot\mathbf{x})\hat{n} + \sin\phi(\hat{n}\times\mathbf{x}) \equiv \hat{R}(\hat{n}, \phi)\mathbf{x}$$

This rotation corresponds to the matrix operator:

$$\hat{R}(\hat{n}, \phi) = \begin{bmatrix} c + (1-c)n_1^2 & (1-c)n_1 n_2 - sn_3 & sn_2 + (1 - cn_1 n_3 \\ (1-c)n_1 n_2 + sn_3 & c + (1-c)n_2^2 & -sn_1 + (1-c)n_2 n_3 \\ -sn_2 + (1-c)n_1 n_3 & sn_1 + (1-c)n_2 n_3 & c + (1-c)n_3^2 \end{bmatrix}$$

where $c = \cos\phi$, $s = \sin\phi$ and $\hat{n} = \hat{n}(n_1, n_2, n_3)$. This matrix can also be written as

$$\hat{R}(\hat{n}, \phi) = \exp\phi(n_1\hat{I}_x + n_2\hat{I}_y + n_3\hat{I}_z)$$

where I_x, I_y, I_z are the infinitesimal generators of the O(3) group, i.e.

$$\hat{I}_x = \begin{bmatrix} 0 & 0 & 0 \\ 0 & 0 & -1 \\ 0 & 1 & 0 \end{bmatrix} \quad \hat{I}_y = \begin{bmatrix} 0 & 0 & 1 \\ 0 & 0 & 0 \\ -1 & 0 & 0 \end{bmatrix} \quad \hat{I}_z = \begin{bmatrix} 0 & -1 & 0 \\ 1 & 0 & 0 \\ 0 & 0 & 0 \end{bmatrix}$$

The equation (21) can now be rewritten as

$$\frac{d\mathbf{X}}{d\Phi} = \alpha(\cos\Phi\hat{I}_z + \sin\Phi\hat{I}_y)\mathbf{X}$$

The transformation (" rotation frame")

$$\mathbf{X}' = \hat{R}(\hat{x}, \Phi)\mathbf{X}$$

eliminates the Φ dependence of the precessional frequency of the vector $\mathbf{X}'$ in the rotating frame since

$$\frac{d\mathbf{X}'}{d\Phi} = \left(\frac{d\hat{R}}{d\Phi}\hat{R}^{-1} + \alpha\hat{R}(\cos\Phi\hat{I}_z + \sin\Phi\hat{I}_y)\hat{R}^{-1}\right)\mathbf{X}' = (\hat{I}_x + \alpha\hat{I}_z)\mathbf{X}'$$

The general solution for $\mathbf{X}'$ is then

$$\mathbf{X}'(\Phi) = \exp\left((\Phi - \Phi_0)(\hat{I}_x + \alpha\hat{I}_z)\right)\mathbf{X}'(\Phi_0)$$

or in the language of rotation matrices,

$$\mathbf{X}'(\Phi) = \hat{R}\left(\frac{1}{\sqrt{1+\alpha^2}}(\hat{n}_1 + \alpha\hat{n}_3), \ (\Phi - \Phi_0)\sqrt{1+\alpha^2}\right)\mathbf{X}'(\Phi_0)$$

The exact solution for $\mathbf{X}(t)$ in the laboratory frame Figure (1) is

$$\mathbf{X}(\Phi) = \hat{R}(\hat{n}_1, -\Phi)\hat{R}\left(\frac{1}{\sqrt{1+\alpha^2}}(\hat{n}_1 + \alpha\hat{n}_3), \ (\Phi - \Phi_0)\sqrt{1+\alpha^2}\right)\hat{R}(\hat{n}_1, \Phi_0)\mathbf{X}(\Phi_0)$$

Initially $\mathbf{X} = \mathbf{X}_i$ when the projectile approaches from infinity so that $\Phi_i = \pi$. The collision is completed when $\Phi_f = \pi$ so that

$$\mathbf{X}_f = \hat{R}\left(\frac{1}{\sqrt{1+\alpha^2}}(\hat{n}_1 + \alpha\hat{n}_3), \ -\pi\sqrt{1+\alpha^2}\right)\hat{R}(\hat{n}_1, \pi)\mathbf{X}_i$$

Upon replacing α by $-\alpha$ the solution $\mathbf{Y}_f$ of the second equation in (20) is

$$\mathbf{Y}_f = \hat{R}\left(\frac{1}{\sqrt{1+\alpha^2}}(\hat{n}_1 - \alpha\hat{n}_3), \ -\pi\sqrt{1+\alpha^2}\right)\hat{R}(\hat{n}_1, \pi)\mathbf{Y}_i$$

These last two equations and the substitutions (19) provide the relations (22) and (23) between the initial and final angular momentum and Runge-Lenz vectors.

REFERENCES

1. Flannery, M. R., *Electron-Ion and Ion-Ion Recombination in Atomic, Molecular and Optical Physics Handbook*, edited by G. W. F. Drake, New York: AIP Press, 1995, ch. 52, pp. 605-629.
2. Kramer, H. A., *Phil. Mag.* **46**, 836 (1923).
3. Stevefelt, J., Boulmer J., and Delpech, J. F., *Phys. Rev. A* **12**, 1246 (1975).
4. Thomson, J. J., *Phil. Mag.* **32**, 419 (1912).
5. Mansbach, P., and Keck, J., *Phys. Rev.* **181**, 275 (1965).
6. Vriens, L., in *Case Studies in atomic collision physics*, edited by E. W. McDaniel and M. K. C. McDowell, New-York: Elsevier, 1969, p. 337.
7. Flannery, M. R., and Vrinceanu, D., [in preparation].
8. Percival, I.C., and Richards, D., *J. Phys. B: Atom. Molec. Phys* **12**, 2051 (1979).
9. Born, M., *The Mechanics of the Atom*, New York: Ungar, 1960, p. 235.
10. Bellomo, P., Farrelly, D., and Uzer, T., *J. Chem. Phys.* **107**, 2499 (1997);
11. Beigman, I. L., and Lebedev, V. S., *Phys. Rep.* **250**, 95 - 328 (1995).

The classical atomic form factor

D. Vrinceanu and M. R. Flannery

School of Physics, Georgia Institute of Technology, Atlanta, Georgia 30332

(January 21, 1999)

The general trends exhibited in the variation of the inelastic form factor in collisional transitions $nl \rightarrow n'l'$, when l' is changed and n, l and n' are kept fixed are explained solely in terms of classical mechanics. Previous quantal results are reproduced from purely classical mechanics principles. Our conclusions are valid not only for large quantum numbers (which provide the usual classical correspondence) but also for other cases, which, up to now have only been described by quantal or semiclassical methods. The interesting trends exhibited in the form factor are directly reflected in experimental and theoretical treatments of collisions involving excited atoms.

32.80.Cy, 34.50.-s, 31.15.Gy

With the advent of new technology which facilitates the accurate measurement [1] of electron - excited atom collision cross section there has also been renewed interest in the theory [2] of collisions involving Rydberg atoms. Recent experiment [1], in particular, has confirmed that the cross section for the quadrupole $2^3S \rightarrow 3^3D$ transition in $e - He(2^3S)$ collisions is much higher then that for the pure dipole $2^3S \rightarrow 3^3P$ transition at low and intermediate energies, in accord with the theoretical predictions of [3] (Born and Multichannel Eikonal approximations). Flannery and McCann [4] have noted that this unexpected behavior is only part of a more general systematic trend in that (a) the $2^3S \rightarrow n^3D$ collisional transitions are predominant over all other transitions to the same value n-value, even for transitions to the electronic continuum and (b) that there is a unique value l'_{max} of the final angular momentum l' that is preferentially populated in $nl \rightarrow n'l'$ transitions $(n' \gg n)$ in collisions between Rydberg atoms and electrons or atoms.

The origin of this general behavior was traced [4] to the variation with l' of the quantum mechanical inelastic form factor

$$\mathcal{F}_{fi}(\mathbf{q}) = \langle \psi_f(\mathbf{r})|e^{i\mathbf{qr}/\hbar}|\psi_i(\mathbf{r})\rangle = \langle \phi_f(\mathbf{p} + \mathbf{q})|\phi_i(\mathbf{p})\rangle \quad (1)$$

for $i(n, l) \rightarrow f(n', l')$ transitions between atomic states; $\psi_{i,f}(\mathbf{r})$ are the wave functions in position space and $\phi_{i,f}(\mathbf{p}) = (2\pi\hbar)^{-3/2} \int \psi_{i,f}(\mathbf{r}) \exp(-i\mathbf{qr}/\hbar)d\mathbf{r}$, the wave functions in momentum space.

When an instantaneous impulse applied at $t = t_0$ transfers momentum $\mathbf{q}$ to an atomic electron, the exact solution of Schrödinger's equation under Hamiltonian

$$H(\mathbf{p}, \mathbf{r}, t) = \mathbf{p}^2/2m - e^2/r - \mathbf{r} \cdot \mathbf{q}\delta(t - t_0) \quad (2)$$

is

$$\Psi(\mathbf{r}, t) = (1 + e^{i\mathbf{qr}/\hbar}\theta(t - t_0))\psi_{nlm}(\mathbf{r})$$

where θ is the Heaviside step function. The probability for $i \equiv |nl\rangle \rightarrow f \equiv |n'l'\rangle$ transitions from the $(2l + 1)$ initial sublevels is then

$$P_{nl,n'l'}(q) = |\langle \psi_{n'l'}|\Psi\rangle|^2 = \sum_{m,m'} |\langle n'l'm'|e^{i\mathbf{qr}/\hbar}|nlm\rangle|^2$$

$$(3)$$

The probability of any impulsive $i \rightarrow f$ transition, whether due to particle collisions or electromagnetic field, is therefore

$$P_{if}(\mathbf{q}) = |\mathcal{F}_{fi}(\mathbf{q})|^2 \quad (4)$$

which provides physical significance to the inelastic form factor, a fundamental property of the atom. For impulsive collisions between a particle 1 and a Rydberg electron 2 bound to a core 3, the overall transition matrix element T decomposes as [5]

$$T_{if}(\mathbf{q}) = \mathcal{F}_{fi}(\mathbf{q})T_{12}(\mathbf{q}) \quad (5)$$

where T_{12}, the matrix element for (1-2) free-free elastic scattering in the (1-2) center of mass, is a function only of $\mathbf{q}$, as for Coulomb scattering $T_{12} = 4\pi\hbar^2 e^2/q^2$, or for Born's approximation, $T_{12} = \int V(\mathbf{r}_{12})exp(i\mathbf{qr}/\hbar)d\mathbf{r}_{12}$. The probability of transition in the target atom per each (1-2) impulsive encounter is $P_{if} = |T_{if}|^2/|T_{12}|^2$, in agreement with (4).

The cross section is obtained by the following integration of the form factor (5) over momentum change,

$$\sigma_{if} = \frac{2\pi}{k_i^2} (M/M_{12})^2 \int_{|k_i - k_f|}^{k_i + k_f} |\mathcal{F}_{fi}(q')|^2 |f_{12}(q')|^2 q'dq' \quad (6)$$

where $k_{i,f}$ are the initial and final wavenumbers of relative motion of the projectile - target system of reduced mass M and $q' = \hbar|\mathbf{k}_i - \mathbf{k}_f|$ is the momentum change. The scattering amplitude for (1-2) collisions of reduced mass M_{12} is $f_{12} = (2M_{12}/4\pi\hbar^2)T_{12}$. For (1-2) slow collisions with scattering length a, the Fermi interaction $V(\mathbf{r}_{12}) = [4\pi a(\hbar^2/M_{12})]\delta(\mathbf{r}_1 - \mathbf{r}_2)$ also yields decomposition (5) with $f_{12} = a$.

The inelastic quantal form factor therefore not only exerts primary importance in collision studies, but also has a deep physical reality. In recent experimental studies of excitation of Rydberg atoms by short unipolar half-cycle electromagnetic pulses the transition amplitude is determined directly by the inelastic form factor [6].

Analytical quantal [7,8] and semiclassical [9] form factors are available although general systematic trends can not be easily extracted from them. A key point of this paper is that a complementary classical approach can also be developed in a way which reveals, quite succintly, important aspects which remain hidden within the quantal treatment.

Consider a Rydberg atom in a stationary (n, l) state with energy E and angular momentum L. If the atom is perturbed by any general impulsive field (as in eq. (2) or the Fermi interaction), then the transition probability to the final state (n', l') (of energy E' and angular momentum L') is the inelastic form factor.

The quantal probability density for finding the electron in the radial interval $(r, r + dr)$ is

$$\rho_{nl}^q(r) = r^2 |R_{nl}|^2 \qquad (7)$$

where R_{nl} is the hydrogenic radial wave function expressed in terms of the generalized Laguerre polynomial.

The phase space of a classical atom, with Hamiltonian $H(\mathbf{r}, \mathbf{p}) = p^2/2m + V(r)$, angular momentum $\mathbf{L}(\mathbf{r}, \mathbf{p}) = \mathbf{r} \times \mathbf{p}$ and period τ_{nl} in stationary state (n, l) is populated according to the microcanonical distribution [10]

$$\rho_{nl}^c \, d\mathbf{r} d\mathbf{p} = \{(2\pi\hbar^2/\tau_{nl})\delta(H - E)\delta(|\mathbf{L}| - L)\} \frac{d\mathbf{r} d\mathbf{p}}{(2\pi\hbar)^3}$$

$$(8)$$

normalized to $(2l + 1)$ states in all of phase space. On integrating over the momentum space $\mathbf{p}$ and angular part of the configuration space $\mathbf{r}$, the classical distribution is

$$\rho_{nl}^c(r) \, dr = \frac{2l + 1}{\tau_{nl}} \frac{2}{\dot{r}} \, dr$$

where the radial speed is given by $m\dot{r}^2/2 = E - V(r) - (l + 1/2)^2\hbar^2/2mr^2$. For the Kepler atom ($\tau_{nl} = 2\pi n^3$ a.u) and ρ_{nl}^c (in a.u.) is

$$\rho_{nl}^c(r) = \frac{1}{\pi n^3} \left[\frac{2}{r} - \frac{1}{n^2} - \frac{(l + 1/2)^2}{r^2} \right]^{-1/2} = \frac{1}{\pi n^3} \frac{1}{\dot{r}(r)}$$

$$(9)$$

The quantal (7) and classical (9) radial probability densities are illustrated in figure Fig. 1. As in the textbook example of the harmonic oscillator, the classical distribution has singularities at the corresponding turning points given by the radii (in a.u.):

$$R^\pm = n^2 \{1 \pm \epsilon\} = n^2 \left\{ 1 \pm \left[1 - (l + 1/2)^2/n^2 \right]^{1/2} \right\}$$

$$(10)$$

The classical distribution is zero outside the accessible region, bounded by $R^\pm$.

By using definition (1) the transition probability (3) can be converted to the new form

$$P_{if}(\mathbf{q}) = (2\pi\hbar)^3 \int \rho_{nl}(\mathbf{r}, \mathbf{p})\rho_{n'l'}^*(\mathbf{r}, \mathbf{p} + \mathbf{q}) \, d\mathbf{r} d\mathbf{p} \quad (11)$$

where the quantal distributions in phase space are given by $\rho^q = (2\pi\hbar)^{-3/2}\psi(\mathbf{r})\exp(-i\mathbf{p} \cdot \mathbf{r}/\hbar)\phi^*(\mathbf{p})$. This form is now suitable for classical correspondence on replacing densities ρ^q by the phase space distributions (8). The basic definition of the classical form factor is therefore given by (8) and (11). The physical significance is that the initial and final state correspond to definite regions in phase space, populated according to the microcanonical distribution (8), and the transition probability is given, in a geometric sense, by the amount of overlap of these regions. In configuration space, the regions are spherical shells with inner and outer radii given by eq. (10), the pericenter (R^-) and apocenter (R^+) of the Kepler orbit.

Analytical expressions with explicit dependence on $\mathbf{q}$ for quantal and classical transition probabilities are developed in a separate paper [8]. Rather than examining the l' variation of (11) for a given q, the key results are more readily deduced and are easily transparent by investigating the probability for all momentum transfers

$$F_{nl \to n'l'}^c = \int P_{if}(\mathbf{q}) \, d\mathbf{q} = (2\pi\hbar)^3 \int_{\mathcal{R}} d\mathbf{r} \, \rho_{nl}^c(\mathbf{r})\rho_{n'l'}^c(\mathbf{r})$$

$$(12)$$

where $\mathcal{R}$ is the overlapping region in configuration space defined by intersection of (R_i^-, R_i^+) and (R_f^-, R_f^+) intervals.

Inserting $\rho(r) = 4\pi\rho^c(r)r^2$ with (9) in (12) gives the classical form factor (CFF)

$$F_{nl \to n'l'}^c = 2\frac{(2l' + 1)}{n^3 n'^3} \int_{R_{min}}^{R_{max}} \frac{dr/r^2}{\dot{r}_i(r)\dot{r}_f(r)} \qquad (13)$$

where $R_{min} = \max(R_i^-, R_f^-)$ and $R_{max} = \min(R_i^+, R_f^+)$ define the bounds of the overlapping region $\mathcal{R}$. Different overlap situations are illustrated in Fig. 2 for a representative case. The gray region is the accessible region for the initial state and the curves are possible final state trajectories. Transitions only occur when the final state trajectory penetrates the initial state accessible region. The longer time spent by the electron on the final state trajectory within the initial state accessible region, the bigger is the transition probability.

2

As l increases from zero to its maximum value for circular orbits, R^- increases from zero to n^2, while R^+ decreases from $2n^2$ to the same value n^2. For final states $n' > \sqrt{2}n$, then $R_{max} = R_i^+$ for all values of l'. Three regions of overlap are then apparent and are respectively accessed as l' is increased:

- *Region I, $R_f^- < R_i^-$:* Here the overlap region $\mathcal{R} \equiv (R_i^-, R_i^+)$ is determined solely by the initial state and has spatial extent which remains constant as l' is varied from zero to some value l_1 where $R_f^- = R_i^-$. There is always an orientation of the final orbit which will then intersect the initial orbit, as exhibited in Fig. 2, for $(n = 3, l = 2)$ and $(n' = 8, l' = 0 - 2)$ orbits. The l' variation of (13) is contained solely within the increasing integrand $(\dot{r}_f)^{-1}$.

- *Region II, $R_i^- < R_f^-$:* Here the overlap region $\mathcal{R} \equiv (R_f^-, R_i^+)$ includes the f-pericenter and has spatial extent which decreases, as l' increases, eventually to zero when $R_f^- = R_i^+$. In this region, the initial and final orbits can intersect each other, as for the $(n' = 8, l' = 4)$ orbit in Fig. 2. The l' variation of (13) results from variation of both the increasing lower limit R_f^- and the increasing integrand $(\dot{r}_f)^{-1}$.

- *Region III, $R_f^- > R_i^+$:* Here the initial and final trajectories no longer intersect, since the pericenter of the final state is greater that the apocenter of the initial state. This region where $(i \rightarrow f)$ transitions do not occur, as illustrated by $(n' = 8, l' = 5, 6, 7)$ orbits in Fig. 2, is the classically inaccessible region.

The boundaries between regions I and II and between regions II and III occur respectively at $l' = l_1$ where $R_f^-(n', l') = R_i^-(n, l)$ and at $l' = l_2$ where $R_f^-(n', l') = R_i^+(n, l)$. Thus l_1 and l_2 are given by

$$(l_{1,2} + \frac{1}{2})^2 = n^2(1 \mp \varepsilon)\left(2 - (1 \mp \varepsilon)n^2/n'^2\right) \quad (14)$$

where ϵ is the eccentricity $[1 - (l + 1/2)^2/n^2]^{1/2}$ of the initial orbit.

Variation of the CFF (13), with final angular momentum l' is then determined both by the lower integration limit R_{min} (which is a constant R_i^- in region I and increases as R_f^- in region II) and by the integrand $(\dot{r}_f)^{-1}$. Fig. 3 illustrates the general pattern. As l' is increased from 0 to l_1 (region I), increase in CFF originates purely from the increasing integrand $(\dot{r}_f)^{-1}$. As l' is varied from l_1 to l_2, the increasing integrand is offset by the decreasing range (R_f^-, R_i^+) of integration (region II). For $l_2 < l' < n - 1$, CFF is zero because transitions are not classically allowed in region III.

At $l' = l_1$ the trajectories touch only at their corresponding pericenters and CFF has a turning point singularity characteristic of classical descriptions. The zero radial speed of the electron at the contact point of both initial and final orbits causes the infinite CFF (transition probability).

As is evident from Figs. 3-5, the agreement between the classical and quantal results is excellent in region I, even for small quantum numbers. In region II, the quantal results oscillate about CFF. Since classical motion is confined to a definite region, the dramatic fall for large l' is more steep than that for the quantal case where states have exponential tails within the classical inaccessible region III. As expected from correspondence principles, for the larger quantum numbers, the quantum form factor tends to CFF, even in the regions II and III, as shown in Fig. 4. The quantal results exhibit maxima in the neighborhood of $l' = l_1, l_2$ where CFF has the classical singularities. The position of l_1 defined by (14) in the limit of large l, where the eccentricity $\varepsilon \rightarrow 0$, is

$$l_1(l \rightarrow n - 1) = n\sqrt{2}(1 - 1/2\,(n/n')^2)^{1/2} - 1/2$$

an exquisite result for initial circular orbits. For $n' \gg n$, l_1 tends from the bottom to

$$l_1(l \rightarrow n - 1, n' \gg n) = n\sqrt{2} - 1/2 \quad (15)$$

a key result in detailed agreement with that previously derived from consideration of the quantal momentum - space overlap [4].

For small initial angular momentum l, $\epsilon \rightarrow 1$ and l_1 is then zero so that the maximum CFF is given by

$$l_2(l \rightarrow 0) = 2n(1 - (n/n')^2)^{1/2} - 1/2$$

appropriate to highly eccentric initial orbits. In the $n' \gg n$ limit then

$$l_2(l \rightarrow 0, n' \gg n) = 2n - 1/2 \quad (16)$$

As the initial l increases, there is therefore a slow variation $(2n \rightarrow \sqrt{2}n)$ in the position of the maximum of CFF (Eq. (15) and (16)), which is pushed slightly to lower values. This theoretical prediction is also confirmed by the quantal results [4].

When the energy E' of the final orbit is not sufficient to accommodate the value of l_2 deduced above $(n' < \sqrt{2}n)$, the peak in CFF (as in Fig. 5) is given by l_1, provided the initial l is large enough. When the final n' is sufficiently small so that the lower l_1 can not be accomodated, i.e. $l_1 > n' - 1$ CFF and the quantal result exhibit a monotonic increase confined to Region I, which is always characterized by excellent agreement between quantal and classical results. Classical expressions (11,13) for the atomic form factor have been derived. The pattern exhibited by the l' variations (Figs. 3-5) is essentially identical with the quantal pattern. The positions of maxima

of the l'-variation of CFF depend strongly on the initial n and only weakly on the initial l, in agreement with the quantal calculations [4], which were restricted to certain cases. Excellent quantitative agreement between classical and quantal results makes the classical form factor a very useful tool particularly at large quantum numbers (Rydberg atoms) where exact quantal results are not easy to obtain (either analytically or numerically) and to use, due to the highly oscillatory nature of the wave function. Although the emphasis here is on the electron form factors, the present analysis is applicable also to form factors for transitions between rovibrational states of molecules.

FIG. 2. Various final state $(n' = 8, l' = 1 - 7)$ trajectories and the initial accessible region corresponding to $(n = 3, l = 2)$.

[1] A. R. Filipelli, C. C. Lin, L. W. Anderson and J. W. McConkey, Adv. At. Mol. Opt. Phys. **33**, 1 (1994); M. E. Lagus, J. B. Boffard, L. W. Anderson and C. C. Lin, Phys. Rev. A **53**, 1505 (1996).

[2] V. S. Lebedev and I. I. Fabrikant, Phys. Rev. A **54**,2888 (1996); M. I. Syrkin, Phys. Rev. A **53**, 825 (1996).

[3] M. R. Flannery and K. J. McCann, Phys. Rev A **12**, 846 (1975);

[4] M. R. Flannery and K. J. McCann, J. Phys. B**12**, 427 (1979); Astrophys. Journ., **236**, 300 (1980).

[5] see e.g. N. F. Mott and H. S. W. Massey, *The theory of atomic collisions*, (Oxford University Press, 1965).

[6] C. O. Reinhold, J. Burgdörfer, R. R. Jones, C. Raman, and P. H. Bucksbaum, J. Phys. B. **28**, L457 (1995).

[7] I. Bersons, and A. Kulsh, Phys. Rev. A **55**, 1674 (1997).

[8] D. Vrinceanu, and M. R. Flannery, *in preparation*.

[9] F. Gounand and L. Petitjean, Phys. Rev. A **30**, 61 (1984).

[10] E. M. Lifshitz and L. P. Pitaevski, *Statistical Physics*, (Pergamon Press, Oxford, 1986).

FIG. 3. Characteristic dependence of the the inelastic form factor on the final angular momentum l', for fixed n (= 3), l (= 2) and n' (= 8). Classical calculations: solid line; quantal results: dots.
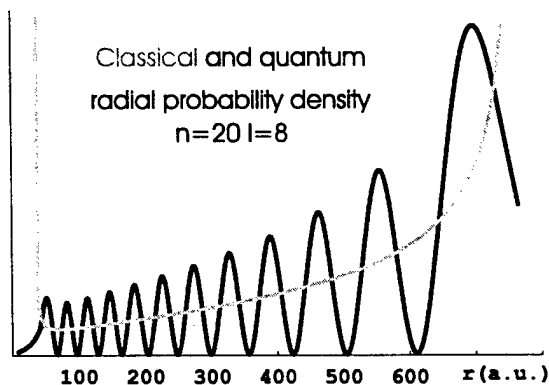

FIG. 1. Classical and quantal radial densities of probability of localization for the stationary state of the hydrogen atom $(E = -1/(2 \times 20^2)$ and $l = 8)$.
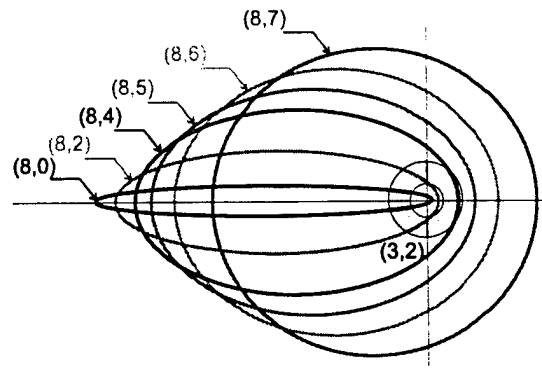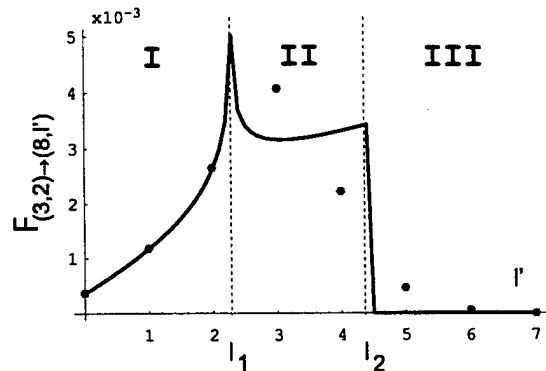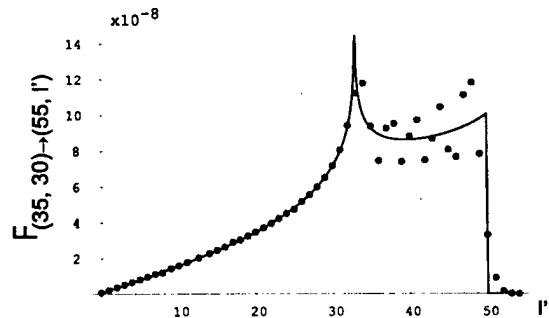

FIG. 4. Classical (solid line) and quantal (dots) inelastic form factor for transitions from state $(n = 35, l = 30)$ to $(n' = 55, l' = 0 \rightarrow 54)$ states.
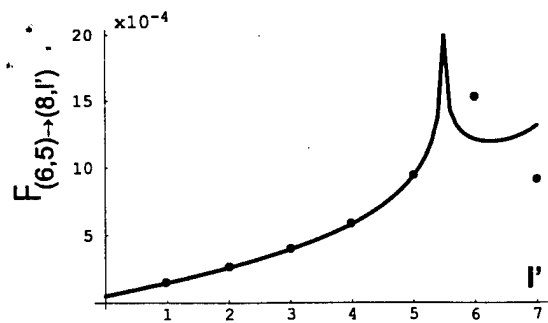
4

FIG. 5. Classical (solid line) and quantal (dots) inelastic form factor for transitions from $n = 6$, $l = 5$ to $n' = 8$ states.

Cross sections for electron excitation of the $2\,^3S$ metastable level of He into higher triplet levels

Garrett A. Piech, Mark E. Lagus, L. W. Anderson, and Chun C. Lin
Department of Physics, University of Wisconsin, Madison, Wisconsin 53706

M. R. Flannery
School of Physics, Georgia Institute of Technology, Atlanta, Georgia 30332
(Received 25 September 1996)

Cross sections for electron excitation out of the $2\,^3S$ metastable level of He into the $2\,^3P$, $3\,^3S$, $3\,^3P$, $3\,^3D$, $4\,^3S$, $4\,^3P$, $4\,^3D$, $5\,^3S$, and $5\,^3D$ levels have been obtained for energies up to 18 eV. We have observed a broad excitation function for the $2\,^3P$ level with a peak apparent cross section of 1.2×10^{-14} cm^2. For the $n=3$, 4, and 5 levels, the excitation functions show a pattern of sharp peaks for excitation into the $n\,^3S$ levels, slightly less sharp peaks for excitation into the $n\,^3P$ levels, and relatively broad peaks for excitation into the $n\,^3D$ levels. Absolute cross sections have been obtained for all the above mentioned levels using a laser-induced fluorescence technique and the results agree well with experimental values reported by Lagus *et al.* [Phys. Rev. A **53**, 1505 (1996)] The cross sections for the $2\,^3S\rightarrow n\,^3P$ excitations which correspond to dipole-allowed optical transitions are smaller than the corresponding $2\,^3S\rightarrow n\,^3S$ and $2\,^3S\rightarrow n\,^3D$ excitation cross sections, in contrast to the trends observed for excitations out of the ground level. This reversal behavior is discussed in terms of the dipole matrix element sum rule. Our cross-section data are compared with those of the alkali-metal atoms. [S1050-2947(97)06204-5]

PACS number(s): 34.80.Dp

I. INTRODUCTION

Excitation out of the metastable levels of rare gases is an important mechanism in a wide variety of phenomena, such as high density gas discharges, astrophysical plasmas, and electron-beam pumped lasers. In the case of the $2\,^1S$ and $2\,^3S$ metastable levels of helium, much theoretical work has been done on calculating both differential and integral cross sections for electron excitation out of these excited levels [1–7]. An early measurement by Gostev *et al.* [8] shows results that are in serious disagreement with the subsequent experiment of Mityureva and Penkin [9]. Measuring cross sections for processes out of the metastable levels has proven to be much more difficult than measuring cross sections for the corresponding processes out of the ground levels of these gases. This is primarily due to the difficulty in producing sufficient densities of metastable atoms to study and separating the associated signal from signals due to ground level atoms. In our laboratory we have used a hollow cathode discharge to produce a thermal atomic beam containing metastable helium with a density of 6×10^7 cm^{-3}. With this apparatus, along with the use of special techniques for detecting very low photon emission signals, we have measured excitation functions and cross sections for electron excitation out of both the singlet and triplet metastable levels for electron energies up to the onset of ground level excitation [10–12]. Our current work represents a refinement and extension into the $n=2$ and $n=5$ triplet levels of the previous results of Rall *et al.* [10]. We have found distinct patterns in the shapes of the excitation functions for the S, P, and D levels.

Part of the motivation for our effort is that the experiment of Rall *et al.*, which used the aforementioned thermal atomic beam as a target, and the experiment of Lagus *et al.* [13], which used a fast (1 keV) beam of metastable atoms produced by charge exchange collisions as a target, had a difference in their absolute cross sections of about 50%. We feel that it is important to improve the absolute calibration of the thermal atomic beam experiment to determine the source of this discrepancy. As discussed in Sec. III E, with the improved absolute calibration our absolute cross-section measurements using the thermal metastable beam target show good agreement with the results of Lagus *et al.*, which are based on an entirely different method of absolute calibration.

II. EXPERIMENTAL APPARATUS

A schematic diagram of our experimental apparatus is shown in Fig. 1, which is quite similar to the apparatus described by Lockwood *et al.* [11,12]. In this experiment, an electron-beam crosses at right angles an atomic beam containing both ground-state and metastable He atoms produced by a hollow cathode discharge. The emission intensity from
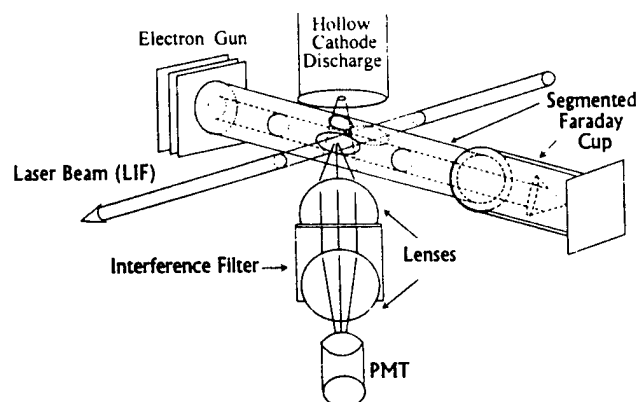

FIG. 1. Schematic diagram of the experimental apparatus used.